J Mater Sci (2007) 42:3537–3543
DOI 10.1007/s10853-006-0582-x

Dynamic formation of zircon during high temperature deformation of zirconia–silica composites with alumina additions

R. Peter Dillon · Martha L. Mecartney

Received: 3 November 2005 / Accepted: 15 June 2006 / Published online: 30 January 2007

Abstract A three phase ceramic composite of 8 mol% Y_2O_3 stabilized ZrO_2 (YSZ), SiO_2, and Al_2O_3 was evaluated for potential high temperature superplasticity. The amorphous SiO_2 content was 5 wt.%, and increasing additions of Al_2O_3 were made. The effect of varying the Y_2O_3 stabilizer concentration in ZrO_2 was also studied. Samples sintered at 1200 °C contained only YSZ, Al_2O_3, and amorphous SiO_2, but $ZrSiO_4$ formed in the samples above 1300 °C. Mullite ($3Al_2O_3 \cdot 2SiO_2$) was not detected in any samples. Specimens of 1 wt.% Al_2O_3–YSZ/SiO_2 had an anomalously high deformation rate of $\sim 2 \times 10^{-4}$ s^{-1} at 1200 °C when compared to YSZ/SiO_2 without Al_2O_3 ($\sim 4 \times 10^{-5}$ s^{-1}). Higher amounts of Al_2O_3 additions decreased the strain rate. Extensive deformation of Al_2O_3 doped YSZ/SiO_2 at 1200 °C induced the formation of $ZrSiO_4$ due to enhanced reaction rates. This distributed, yet locally interconnected, zircon phase rapidly eroded the strain rate after ~60% deformation.

Introduction

Reports that 390% tensile strain can be achieved in 4 s at 1650 °C for a three phase zirconia–alumina–spinel ceramic composite demonstrated the advantages of using a three phase system for enhancing superplastic behavior in ceramics [1]. Grain growth is severely constrained by second and third phases [1] and the fine grain microstructure required for superplastic deformation is maintained [2]. Superplasticity may be further enhanced by cations supplied from the additional phases which enhance diffusion along the ZrO_2 grain boundaries [3].

The purpose of this study is to investigate the use of this three-phase concept in a high zirconia volume ceramic composite containing both glassy and crystalline second phases. The goal is to produce a uniform fine grain microstructure with enhanced high temperature deformability using nanocrystalline Al_2O_3 powder and colloidal SiO_2. Separately, each of the phases have been shown previously to be highly effective in enhancing the high temperature ductility of 8 mol % yttria cubic stabilized zirconia (8Y-CSZ) [4–8]. Our hypothesis was that the addition of both Al_2O_3 and SiO_2 would result in a synergistic improvement in high temperature deformability. In this current study zirconia/5 wt. % SiO_2 materials with varying amounts of Al_2O_3 and Y_2O_3 stabilizer were used to study phase formation and high temperature deformation.

Experimental procedure

Sample preparation

Commercially available 8Y-CSZ (TZ-8Y—Tosoh, Japan; Y_2O_3: 13.24 wt.%, Al_2O_3: 0.006 wt.%, SiO_2: 0.004 wt.%, Fe_2O_3: 0.004 wt.%, Na_2O: 0.070 wt.%) powder and colloidal SiO_2 (Nissan Chemicals, NY) were used in combination with α-Al_2O_3 (Baikalox CR30F—Baikowski, NC; Ca: 1.5 ppm, Fe: 2.8 ppm,

R. P. Dillon · M. L. Mecartney (✉)
Department of Chemical Engineering and Materials Science, University of California, Irvine, CA 92697-2575, USA
e-mail: martham@uci.edu

K: 22 ppm, Na: 17 ppm, Si: 17 ppm) powder. Five ceramic powder blends (Table 1) with varying amounts of Al_2O_3 were produced by attritor-milling with 3Y-TZP milling balls. The slurry of the ceramic components and isopropanol were dried overnight at 120 °C, crushed and sieved to <80 μm.

In order to investigate the effects of yttria, two additional ceramic powder blends, also listed in Table 1, were produced by attritor-milling. 3Y-TZP milling balls were used for 3YSZ-5S-1A and alumina milling balls were used for Z-5S-1A to minimize contamination.

Specimens were prepared by consolidating the appropriate blend by cold isostatic pressing at 400 MPa followed by sintering (1200 °C, 1300 °C, or 1450 °C) for 3 h. All compression test specimens were sintered at 1200 °C for 3 h to produce dense cylindrical specimens approximately 6 mm in height and 3 mm in diameter. With the exception of the sample prepared with pure zirconia powder, all samples were >98% dense after sintering as determined by the Archimedes method and assuming a microstructure comprised of the constituent phases of yttria stabilized zirconia (YSZ), alumina, and silica. The sample prepared with pure zirconia powder and 5 wt.% SiO_2 + 1 wt.% Al_2O_3 was ~97% dense as determined by Archimedes method.

Microstructural characterization

The crystalline phases of the samples were determined by X-ray diffraction (XRD) using a Siemens D5000 X-ray diffractometer using CuKα radiation. The microstructural morphology was revealed by polishing and thermally etching at 1200 °C for 0.5 h and observed using the back-scattered electron mode in a Philips XL30 FESEM. This technique allowed the capture of high contrast images due to the difference in back-scatter electron yield from 8Y-CSZ (light gray in the images), $ZrSiO_4$ (medium gray), and the glassy SiO_2 (residing at multi grain junctions) and crystalline Al_2O_3 (dark gray or black). Grain size measurements were performed using Scion Image, image analysis software. Uncorrected grain diameters were calculated from the cross sectional areas of the defined grains. The ''three dimensional'' grain size was obtained by multiplying the measured values by a correction factor of 1.74 [9].

Table 1 Primary ceramic mixtures investigated

Designation	8Y-CSZ		Al_2O_3		SiO_2	
	wt.%	Vol.%	wt.%	vol.%	wt.%	vol.%
8YSZ-5S	95	87.4	0	0	5	12.6
8YSZ-5S-1A	94	86.1	1	1.4	5	12.5
8YSZ-5S-3A	92	83.5	3	4.1	5	12.4
8YSZ-5S-5A	90	80.9	5	6.8	5	12.3
8YSZ-5S-10A	85	74.7	10	13.3	5	12.0
3YSZ-5S-1A	94 wt. % 3Y-TZP		1		5	
Z-5S-1A	94 wt. % ZrO_2		1		5	

Compression testing

High temperature compression tests were performed on the compression samples at 1200 °C for 3 h in a compression creep furnace (ATS, Inc. PA) between two SiC rods under a constant stress of 30 MPa. Constant stress was maintained throughout the experiments by monitoring the sample displacement throughout the test, calculating the change in cross sectional area, assuming a uniform diameter throughout the samples, as the sample height changed, and adjusting the load to compensate for the increasing cross-sectional area. Such adjustments were made at intervals of ~0.025 strain. For all experiments the creep furnace reached the testing temperature in 3 h.

Results

Microstructure of Sintered Samples

Figure 1 illustrates the change in microstructure due to varying either the sintering temperature or Al_2O_3 content for 8YSZ containing 5 wt.% (12.6 vol.%) SiO_2. All compositions sintered at 1200 °C are fine grained with SiO_2 glass distributed fairly uniformly at multi-grain junctions. Al_2O_3 could only be detected in specimens containing 3 wt.% or more Al_2O_3. The average initial grain size and standard deviation of the grain size distribution of zirconia for the specimens sintered at 1200 °C are summarized in Table 2. XRD of these samples shows only crystalline 8Y-CSZ and Al_2O_3 present (Fig. 2). Al_2O_3 is detected by XRD in the samples containing 5 or greater wt.% Al_2O_3. No other phases were detected by XRD for samples sintered at 1200 °C. (Amorphous SiO_2 is not detected by XRD).

Sintering 8Y-CSZ with 5 wt.% SiO_2 without Al_2O_3 at temperatures higher than 1200 °C results in grain growth (compare Fig. 1a, e), but no new phases form. In contrast, significant morphological changes are

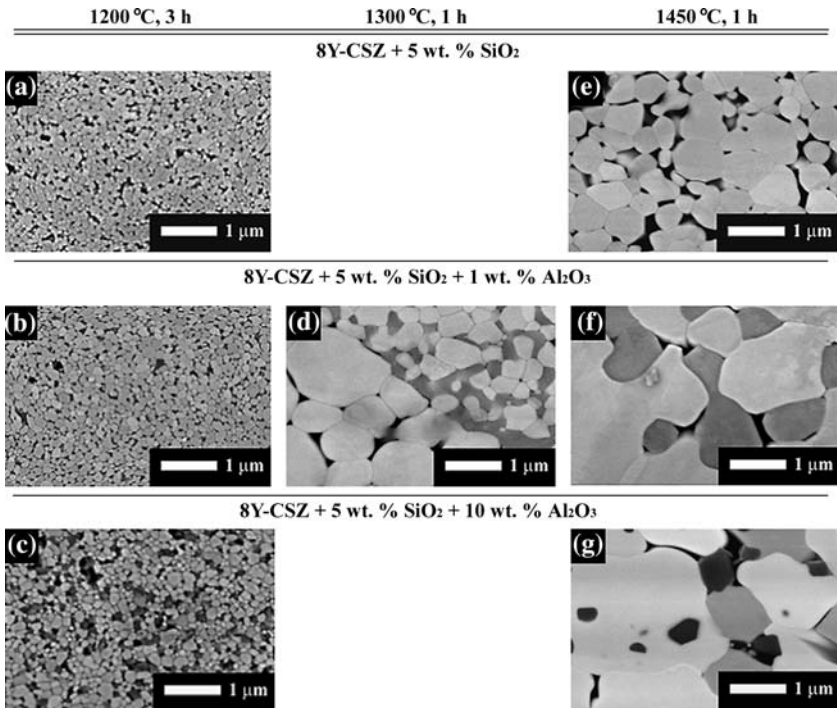

Fig. 1 Microstructural variation resulting from varying sintering temperature and alumina concentration. **(e)** shows white grains of 8Y-CSZ and dark regions of intergranular SiO_2; (**f**) shows white grains of 8Y-CSZ and gray regions of crystallized $ZrSiO_4$; (**g**) shows white grains of 8Y-CSZ, gray regions of $ZrSiO_4$, and black particles of Al_2O_3

Table 2 8Y-CSZ grain size and standard deviation before and after deformation at 1200 °C for 3 h for 8Y-CSZ with 5 wt.% SiO_2 and various amounts of Al_2O_3

Material	Initial Grain Size (μm)	Final Grain Size (μm)
8YSZ-5S	0.20 ± 0.08	0.24 ± 0.14
8YSZ-5S-1A	0.29 ± 0.10	0.41 ± 0.18
8YSZ-5S-3A	0.28 ± 0.10	0.50 ± 0.21
8YSZ-5S-5A	0.24 ± 0.09	0.53 ± 0.19
8YSZ-5S-10A	0.26 ± 0.09	0.64 ± 0.33

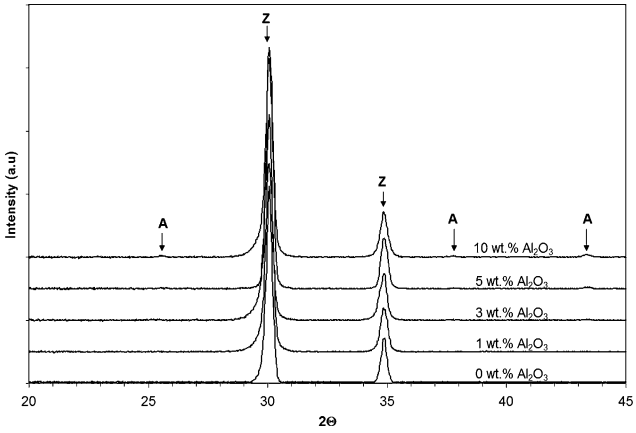

Fig. 2 X-ray diffraction patterns for 8Y-CSZ + 5 wt.% SiO_2 with varying amounts of Al_2O_3 prior to deformation. Specimens were sintered at 1200 °C for 3 h. **Z** = 8Y-CSZ. **A** = Al_2O_3

observed in Al_2O_3 containing specimens if sintered above 1200 °C (compare Fig. 1f, g). A third crystalline phase appears at 1300 °C within a network of large 8Y-CSZ grains. This new phase is $ZrSiO_4$ as determined by XRD (Fig. 3). At 1300 °C, this phase is inhomogeneously present across the sample with regions of 8Y-CSZ and intergranular silica existing next to regions of 8Y-CSZ and crystalline zircon (Fig. 1d).

Compression testing

High temperature deformation tests of ceramic composite samples with varying amounts of Al_2O_3 are presented in Fig. 4. Tests were conducted at 1200 °C, below the temperature observed for the

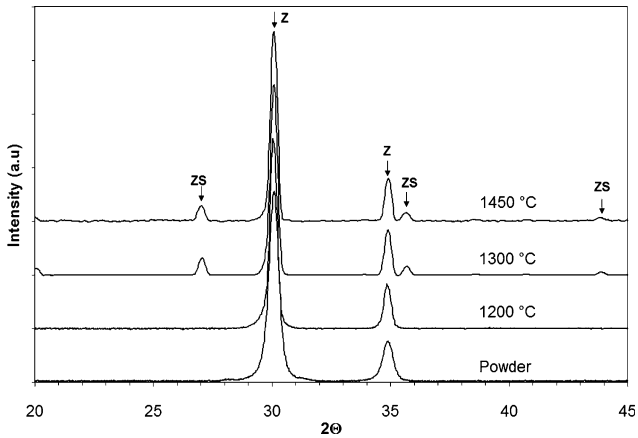

Fig. 3 X-ray diffraction patterns for 8Y-CSZ + 5 wt.% SiO_2 + 1 wt.% Al_2O_3. The specimen at 1200 °C was sintered for 3 h; all others were sintered for 1 h. **Z** = 8Y-CSZ. **ZS** = $ZrSiO_4$

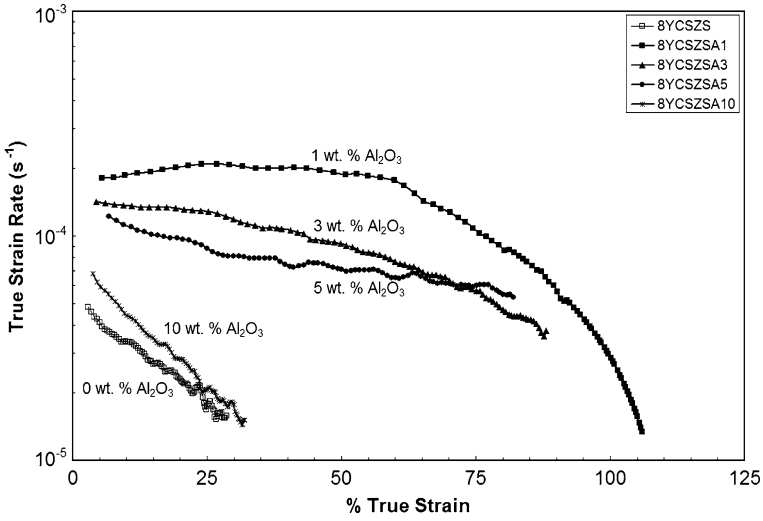

Fig. 4 Compression deformation at 1200 °C for Al_2O_3 doped 8Y-CSZ + 5 wt.% SiO_2 as a function of Al_2O_3 content. Constant applied stress of 30 MPa

formation of $ZrSiO_4$ during sintering. A high initial strain rate of $\sim 2 \times 10^{-4}$ s^{-1} was observed in the sample with 1 wt.% Al_2O_3, 8 times faster than the sample with only 8Y-CSZ + 5 wt.% SiO_2. The strain rate decreased with increasing amounts of Al_2O_3. The strain rate was only slightly higher in the sample containing 10 wt.% Al_2O_3 compared to the sample containing no Al_2O_3. The 1 wt.% Al_2O_3 sample was the only sample to exhibit nearly steady state deformation until ~60% true strain, after which there was a rapid decrease in strain rate.

Microstructural observations of alumina containing samples after deformation revealed the presence of inhomogeneously distributed reaction zones (Fig. 5a). Zircon formed between the silica glass pockets and 8Y-CSZ grains (Fig. 5b). XRD of samples after deformation at 1200 °C for 3 h, (Fig. 6), indicates the formation of zircon in alumina containing specimens, while no zircon was detected in the specimen without alumina (Fig. 6). The (200) zircon peak in the 10 wt.% Al_2O_3 sample was barely detectable. This sample exhibited slightly more than 30% strain, the least amount of strain for the Al_2O_3 containing samples. The average grain size and standard deviation of the grain size distribution of zirconia after deformation are summarized in Table 2. With increasing Al_2O_3 content, the average grain size of YSZ increased.

The role of yttria on the deformation of zirconia/SiO_2 + 1 wt.% Al_2O_3 is shown in Fig. 7. The high temperature deformation of 8YSZ with 5 wt.% SiO_2 and 1 wt.% Al_2O_3 is compared with samples of similar composition made with 3 mol% yttria stabilized tetragonal zirconia polycrystal (3Y-TZP) and pure ZrO_2. 3Y-TZP shows further strain rate enhancement (~75% greater) compared to that observed in

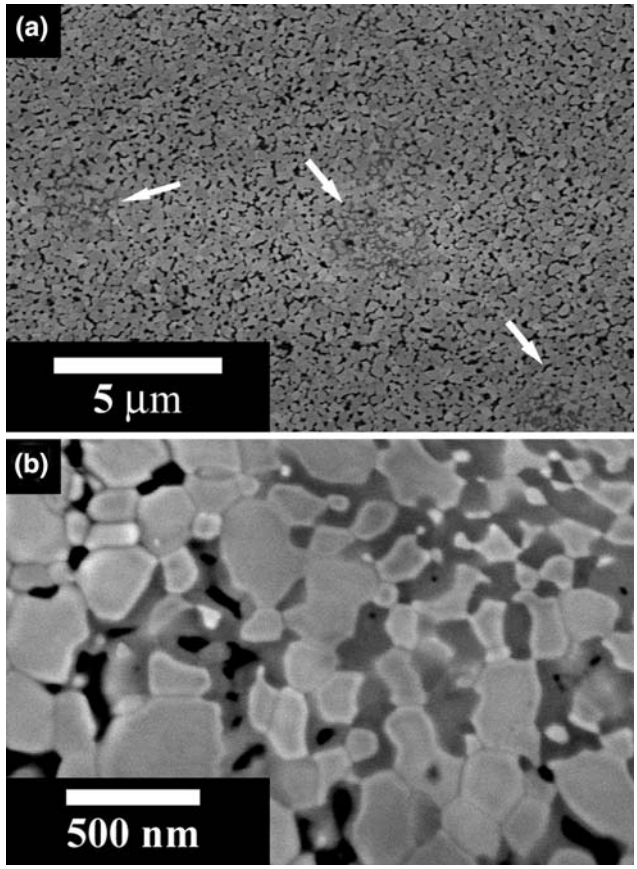

Fig. 5 Formation of $ZrSiO_4$ after deformation of 8Y-CSZ/SiO_2 with 1 wt.% Al_2O_3. (**a**) Inhomogeneous crystallization of $ZrSiO_4$. (**b**) Reaction between 8Y-CSZ and SiO_2. Light gray is 8Y-CSZ, gray is $ZrSiO_4$, and black is SiO_2

8YSZ-5S-1A. Both the 8Y and 3Y samples showed a marked decrease in strain rate with large deformations. XRD analysis of the pure ZrO_2 with 5 wt. % SiO_2 and

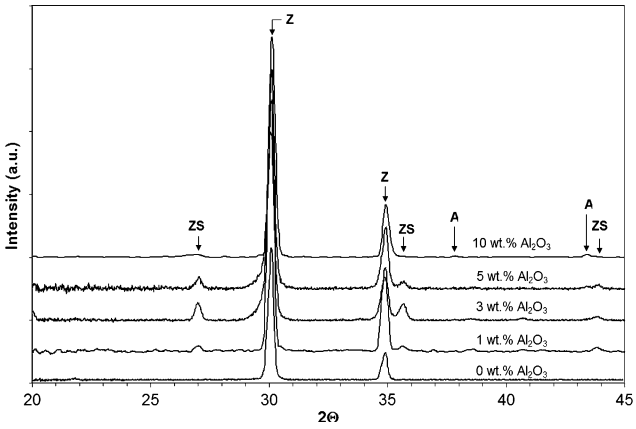

Fig. 6 X-ray diffraction patterns for 8Y-CSZ + 5 wt.% SiO_2 with various concentrations of Al_2O_3 after deformation at 1200 °C. Specimens were previously sintered at 1200 °C for 3 h. **Z** = 8Y-CSZ. **A** = Al_2O_3. **ZS** = ZrSiO4

1 wt.% Al_2O_3 sample after deformation at 1200 °C for 3 h also showed the formation of zircon after deformation.

Discussion

The expected strain rate for 8Y-CSZ + 5 wt.% SiO_2 at 1200 °C, determined by extrapolating Sharif and Mecartney's [7] compression deformation results, is ~1×10^{-5} s^{-1}. Compensating for the difference in initial grain size (strain rate $\propto d^{-p}$ where d is the average grain size and p is the grain size exponent which is assumed to be 2 here), the expected strain rate should be ~6×10^{-5} $^{-1}$. This agrees well with the observed initial strain rate of ~5×10^{-5} s^{-1} in Fig. 4. Re-evaluation of Sharif and Mecartney's [7] compression deformation data considering a change in the average grain size from 0.20 μm to 0.24 μm predicts a strain rate of ~3.5×10^{-5} s^{-1}. The observed decrease in strain rate to ~1.5×10^{-5} s^{-1} is still reasonably close to the predicted value (within experimental error) suggesting grain growth controls the strain rate in 8Y-CSZ + 5 wt.% SiO_2.

The increased strain rate at constant stress for Al_2O_3 containing specimens as compared to the undoped sample (Fig. 4) is similar to observations of decreased flow stress at a constant strain rate in previous studies of alumina doped 3Y-TZP zirconia–silica ceramic glass composites [10–12]. Direct comparisons to these studies may be misleading since the alumina composition in those studies was limited to at most 1/10 that used in the present study. However, Al^{3+} segregation at zirconia grain boundaries described in previous studies [10–12] should have the same effect of enhancing grain boundary diffusion in this system. Enhanced aluminum cation diffusion and aluminum segregation to zirconia grain boundaries has been used to explain increased sinterability [13], accelerated grain growth [14], and increased ductility [15] of SiO_2–ZrO_2 doped with Al_2O_3.

The grain size of deformed specimens (Table 2) is a combination of dynamic and static grain growth. There is significantly more grain growth of YSZ for alumina containing specimens. Despite an increase in grain size, the highest strain rate was observed for 1 wt.% Al_2O_3 containing specimens compared to samples without Al_2O_3 (Fig. 4). Approximately 1 wt.% is the solubility limit reported for Al_2O_3 in 8Y-CSZ [16], suggesting nearly complete dissolution of Al_2O_3 in these specimens and the important role of aluminum cations in enhancing deformation in this system.

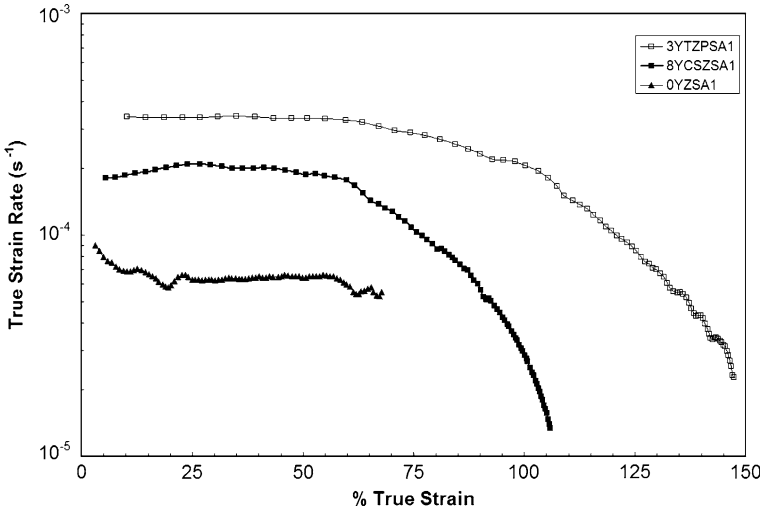

Fig. 7 Compression deformation in 1 wt.% Al_2O_3 doped ZrO_2 as a function of Y_2O_3 concentration. All samples contain 5 wt.% SiO_2 and were deformed 3 h under 30 MPa at 1200 °C

The rapid decrease in strain rate after ~65% true strain for 1 wt.% Al_2O_3 samples is caused by the formation of localized regions of interconnected $ZrSiO_4$ (Fig. 5) which ''lock up'' the microstructure. Zircon forms as a reaction between the ZrO_2 grains and SiO_2 pockets. The expected strain rate in zircon at 1200 °C, determined by scaling Goretta et al.'s [17] compression deformation results and using their value of $n = 1.1$, is $\sim 8 \times 10^{-7}$ s^{-1}. This is still more than an order of magnitude less than the observed $\sim 1 \times 10^{-5}$ s^{-1} strain rate following deformation to 105% true strain in 8Y-CSZ/SiO_2 + 1 wt.% Al_2O_3. The strain rate should further decrease with continued deformation as a significant amount of glass is still available for zircon formation (Fig. 5a).

The relevant phase diagrams [18, 19] show two ternary eutectics, 1539 °C for ZrO_2–Al_2O_3–SiO_2 [18] and 1371 ± 5 °C for Y_2O_3–SiO_2–Al_2O_3 [19], so no significant amount of transient liquid phases are expected to form at the deformation temperature of 1200 °C. The formation of mullite is thermodynamically preferable to the formation of $ZrSiO_4$ from the reactants Al_2O_3, SiO_2, and ZrO_2 [20]. However, $ZrSiO_4$ is present in all the deformed alumina-containing specimens and it is not found in deformed 8Y-CSZ/SiO_2 without Al_2O_3. Yaroshenko and Wilkerson [20] suggest that mullitization in ZrO_2–Al_2O_3–SiO_2 is a two step process where the intermediate formation of zircon provides a lower energy route to the formation of mullite than a single step reaction. Metastable zircon formation is expected up to ~1475 °C [20]. Based on the greater solubility of Al_2O_3 compared to SiO_2 in ZrO_2, Kanno [21] suggests Al_2O_3 is more effective in activating a reactive surface layer in ZrO_2 than SiO_2. Enhanced grain boundary diffusivity, as a result of the dissolution of Al_2O_3, may also assist the formation of zircon during deformation in this current study.

The deformation behavior for specimens with increasing amounts of Al_2O_3 (Fig. 4) is dominated by a lower initial strain rate with increasing Al_2O_3 content due to the increased volume fractions of second phase Al_2O_3 [5, 22]. The limited amount of $ZrSiO_4$ detected in the deformed specimen containing 10 wt.% Al_2O_3 (Fig. 6) illustrates the role of deformation, assisting the formation of $ZrSiO_4$ in this system. This specimen with its minimal (200) $ZrSiO_4$ peak did not exceed 35% true strain in 3 h at 30 MPa. More pronounced (200) $ZrSiO_4$ peaks are exhibited in all other Al_2O_3 containing specimens which were deformed to a greater extent, over 60% true strain. This suggests a certain amount of deformation enhanced diffusion is required to form $ZrSiO_4$ in this system at 1200 °C.

Figure 7 illustrates the deformation behavior of ZrO_2/SiO_2/Al_2O_3 with ranges of Y_2O_3 contents. The initial non-linear portion of the creep curve for the specimen containing pure zirconia (Fig. 7) is due to densification of the sample required due to the monoclinic to tetragonal phase transformation upon heating. The lower strain rate of this specimen may be explained by the larger initial grain size of pure ZrO_2. $ZrSiO_4$ is also formed in the pure ZrO_2 sample after deformation as found by XRD. The fine and more stable grain size of 3Y-TZP contributes to the higher strain rate for the material, but similar to the 8Y-CSZ based material, the deformation rate degrades after a period of steady-state deformation, albeit at a later point than 8Y-CSZ. Y_2O_3 can act as a sintering additive and lower the activation barrier for nucleation of $ZrSiO_4$ [20]. In this study Y_2O_3 is not required to form $ZrSiO_4$ in the presence of Al_2O_3 and with high temperature deformation.

While the dynamic formation of zircon during deformation of YSZ/SiO_2 with alumina is the focus for this paper, the locking microstructure developed from the transient silica phase (Fig. 8) offers some advantages [23]. Low temperature net shape forming with amorphous silica could be used to fabricate complex shapes. A subsequent higher temperature heat treatment would react ZrO_2 and SiO_2 to form a contiguous zircon phase making the final material useful for high temperature applications. If care is taken to eliminate any residual glass, the creep resistance of the zircon phase might rival that of mullite [17].

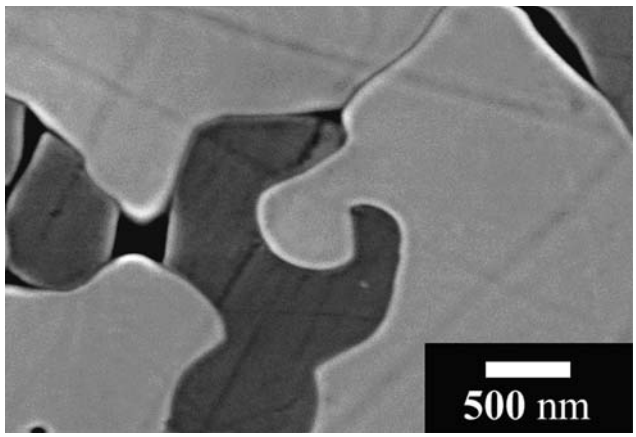

Fig. 8 Locking microstructure of $ZrSiO_4$ (dark gray) and 8Y-CSZ (light gray) formed after high temperature heat treatment of 1450 °C, 1 h

Conclusion

High temperature ductility (~1200 °C) is enhanced in 8Y-CSZ + 5 wt.% SiO_2 by the addition of Al_2O_3. The highest strain rate of 2×10^{-4} s^{-1} at 1200 °C occurs with the addition of ~1 wt.% Al_2O_3. Extensive deformation induces the formation of $ZrSiO_4$ in SiO_2/Al_2O_3 doped 8Y-CSZ. This is most likely the result of increased grain boundary diffusivity during deformation. The formation of $ZrSiO_4$ is largely responsible for a change from steady-state to a rapidly decreasing strain rate due to localized regions of interconnected $ZrSiO_4$ in samples with 1wt.% Al_2O_3. Decreased strain rates of the specimens with increasing Al_2O_3 content is due to increasing flow stresses as more Al_2O_3 is present as a second phase.

Acknowledgements This work was supported by the National Science Foundation under Grant No. DMR-0207197.

References

1. Kim BN, Hiraga K, Morita K, Sakka Y (2001) Nature 413:288
2. Chen I-W, Xue LA (1990) J Am Ceram Soc 73:2585
3. Morita K, Hiraga K, Kim BN, Sakka Y (2004) Mater Trans 45:2073
4. Sharif AA, Mecartney ML (2004) J Eur Ceram Soc 24:2041
5. Suzuki TS, Sakka Y, Morita K, Hiraga K (2000) Scripta Mater 43:705
6. Kajihara K, Yoshizawa Y, Sakuma T (1995) Acta Metall Mater 43:1235
7. Sharif AA, Mecartney ML (2003) Acta Mater 51:1633
8. Dillon RP, Sosa SS, Mecartney ML (2004) Scripta Mater 50:1441
9. Thompson AW (1972) Metallography 5:366
10. Ikuhara Y, Yoshida H, Sakuma T (2001) Mater Sci & Eng A A319-321:24
11. Sakuma T, Ikuhara Y, Takigawa Y, Thavorniti P (1997) Mater Sci & Eng A A234-236:226
12. Thavorniti P, Ikuhara Y, Sakuma T (1998) J Am Ceram Soc 81:2927
13. Hassan AAE, Menzler NH, Blass G, Ali ME, Buchkremer HP, Stover D (2002) J Mater Sci 37:3467
14. Chokshi AH, Yoshida H, Ikuhara Y, Sakuma T (2003) Mater Lett 57:4196
15. Sakka Y, Ishii T, Suzuki TS, Morita K, Hiraga K (2004) J Eur Cer Soc 24:449
16. Feighery AJ, Irvine JTS (1999) Solid State Ionics 121:209
17. Goretta KC, Cruse TA, Koritala RE, Routbort JL, Melendez-martinez JJ, De Arellano-Lopez AR (2001) J Eur Ceram Soc 21:1055
18. Ondik HM, Mcmurdie HF (eds) (1998) Phase diagrams for zirconium and zirconia systems. The American Ceramic Society, Westerville, p. 254
19. Kolitsch U, Seifert HJ, Ludwig T, Aldinger F (1999) J Mater Res 14:447
20. Yaroshenko V, Wilkinson DS (2000) J Mater Res 15:1358
21. Kanno Y (1989) J Mat Sci 24:2415
22. Sakka Y, Suzuki TS, Morita K, Nakano K, Hiraga K (2001) Scripta Mater 44:2075
23. Xue LA, Chen I-W (1992) J Am Ceram Soc 75:1085